ACS Catalysis

Research Article

Cite This: ACS Catal. 2018, 8, 11987−11998

pubs.acs.org/acscatalysis

Catalytic Consequences of Reactive Intermediates during CO Oxidation on Ag Clusters

Petar T. Lachkov and Ya-Huei Cathy Chin*

Department of Chemical Engineering and Applied Chemistry, University of Toronto, Toronto, Ontario M5S 3E5, Canada

Supporting Information

ABSTRACT: Kinetic measurements, microkinetic modeling, and CO and O_2 uptake experiments lead to a proposed mechanism for CO oxidation on dispersed Ag cluster surfaces. CO turnovers occur via kinetically relevant reactions between O_2* and CO* on Ag cluster surfaces nearly saturated with O* and CO*. The operating pressure ratio of O_2 to the square of CO, $[O_2]$-to-$[CO]^2$, dictates the relative O* and CO* coverages and in turn the rate coefficients. Low $[O_2]$-to-$[CO]^2$ ratios lead to Ag cluster surfaces saturated with CO*, during which the first-order rate coefficients ($r_{CO}[CO]^{-1}$) increase linearly with the pressure ratio. As the $[O_2]$-to-$[CO]^2$ ratio increases, the CO* coverages decrease and O* coverages concomitantly increase, and the rate coefficients become independent of the $[O_2]$-to-$[CO]^2$ ratio. CO* binds to Ag clusters more strongly than O*, and as a result, CO* coverages decrease and O* coverages increase as the reaction temperature rises when comparing at a constant $[O_2]$-to-$[CO]^2$ ratio. The rate coefficients for CO oxidation on CO* covered Ag clusters initially increase with increasing Ag cluster diameter to ∼5 nm, but decrease with a further increase in Ag diameter beyond 5 nm. The former trend reflects more weakly bound and reactive O_2* and CO*, and the latter likely reflects the depletion of O_2* molecules.

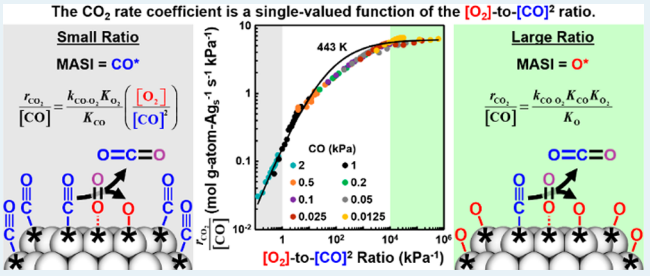

KEYWORDS: *carbon monoxide, oxidation, chemisorbed oxygen, oxygen coverage, Ag cluster, temperature effect, activation barrier, structure sensitivity effect*

1. INTRODUCTION

Catalytic CO oxidation is of practical relevance for automobile exhaust emission controls[1−3] and the removal of CO impurities from the hydrogen feed stream of proton exchange membrane (PEM) fuel cells.[4−6] The simple reaction occurs on metal surfaces and involves the activation of O_2, kinetically coupled with the insertion of an oxygen atom into a CO molecule.[7−12] The catalytic steps, their kinetic relevance, and the coverages of surface intermediates are known to vary with the operating temperature,[11] reactant pressures,[7] and metal identity of the catalyst.[13,14] For these reasons, the reaction exhibits complex kinetic behavior with diverse kinetic dependencies.

CO oxidation reactions on Pd {(100)[8] and (111)[9] surfaces} and Pt {1.2−25 nm clusters[10,11,15]} occur on surfaces covered with adsorbed CO molecules (CO*, where "*" denotes a metal site) to different extents, depending on the CO and O_2 pressures and reaction temperature. On these metals, CO turnover rates at moderate temperatures (358−500 K) are inversely proportional to CO pressures and increase linearly with O_2 pressures.[8−10] Under these conditions (358 K), infrared (IR) spectroscopic studies on Pt clusters show that CO* nearly saturates the cluster surfaces. Specifically, the absorption band intensities for the linearly adsorbed CO* at 2070−2090 cm^{-1} remain unaltered with changing CO pressure (0.09−0.15 kPa).[10] On such surfaces, the measured rate dependencies would suggest that the kinetically relevant step is either the surface reaction between O_2* and CO* or the O_2 activation at a vacant metal site (*) assisted by vicinal CO*. Density functional theory (DFT) studies modeled the CO* assisted O_2 activation on a cuboctahedral Pt cluster containing 201 Pt atoms, nearly saturated with CO* and containing a single vacancy and reported an activation barrier of 94 kJ mol^{-1} on its (111) terraces, which is consistent with the measured value of 84 kJ mol^{-1} on 1.2−20 nm Pt clusters.[10] These kinetic, infrared, and DFT methods suggest that CO adsorption is quasi-equilibrated and that O_2 activation at a metal site is assisted by a vicinal CO*; the latter is the kinetically relevant step for CO oxidation on Pt clusters.

In contrast to Pt and Pd, CO oxidation reactions on Ru, Rh, Ir, and Au {Ru(0001),[7] Rh(111),[7] Ir(111),[16] and 4−8 nm Au clusters supported on Ce_3O_4, Fe_2O_3, or TiO_2[17]} at moderate temperatures (273−525 K) occur on metal surfaces covered with both CO* and O*, depending on the metal identity and CO and O_2 pressures. Reactions on Ru(0001),[7] Rh(111),[7] and Ir(111)[16] exhibit two distinct kinetic regimes (regimes 1 and 2), each with unique rate dependencies, defined by the operating reactant pressure ratios. In regime 1, which prevails at high CO and low O_2 pressures {e.g., Ru(0001): 2.1 kPa CO, 0.06−0.26 kPa O_2, 500 K;[7] Rh(111): 2.1 kPa CO, 0.5−13 kPa O_2, 500 K;[7] Ir(111):

Received: May 4, 2018
Revised: October 10, 2018
Published: October 26, 2018

DOI: 10.1021/acscatal.8b01760
ACS Catal. 2018, 8, 11987−11998

0.37−8.1 kPa CO, 2.7 kPa O_2, 525 K[16]}, turnover rates are inversely proportional to CO and increase linearly with O_2 pressures, identical to those observed on Pd[8,9] and Pt.[10,11,15] In regime 2, which occurs at lower CO pressures and/or higher O_2 pressures {e.g., Ru(0001): 2.1 kPa CO, 0.51−21 kPa O_2, 500 K;[7] Rh(111): 2.1 kPa CO, 33−65 kPa O_2, 500 K;[7] Ir(111): 0.022−0.22 kPa CO, 2.7 kPa O_2, 525 K[16]}, turnover rates begin to increase linearly with CO pressures and remain invariant with O_2 pressures. This distinct transition in kinetic dependencies may reflect a change in the most abundant surface intermediates from CO* to O*, while the CO* assisted O_2 activation reaction remains as the kinetically relevant step. In fact, Auger electron spectroscopy (AES) measurements of the O 1s core hole formation (510 eV) confirm an increase in the surface oxygen contents on Ru(0001) with increasing O_2 pressure (0.064−0.53 kPa) during CO−O_2 reactions at a constant CO pressure and 500 K.[7] The change in O* concentration corresponds to a transition from negligible to monolayer (ML) O* coverages at the Ru(0001) surfaces, and this change coincides with the observed kinetic transition. Lastly, CO oxidation turnover rates on Au clusters (2−18 nm)[17] exhibit rate dependencies between zero and first order in CO and O_2 pressures over a wide range of conditions (0.1−10 kPa CO, 0.4−20 kPa O_2) at 273 K. These results suggest that Au surfaces are only partially covered with CO* and/or O*, which likely stems from the much smaller heats of CO* or O* adsorption and thus the concomitantly smaller affinities of these molecules to Au than other metals (Ru, Rh, Ir, Pd, and Pt).

These complex rate dependencies on the series of metals appear to reflect a change in the identity of the most abundant surface intermediates among these metals, as they catalyze the CO oxidation reaction. For each metal, the relative O* and CO* site coverages appear to correlate with the difference in its heats of O* and CO* adsorption, ΔQ_{O-CO}:

$$\Delta Q_{O-CO} = Q_{ads,O} - Q_{ads,CO} = -\Delta H_{ads,O} - (-\Delta H_{ads,CO}) \quad (1)$$

where $Q_{ads,j}$ is the heat of adsorption for species j (j = O* or CO*), which also equals the negative of the adsorption enthalpy for species j {$\Delta H_{ads,j}$; where j = O* for the adsorption step $1/2(O_2 + 2* \rightarrow 2O*)$ or j = CO* for the adsorption step $CO + * \rightarrow CO*$}. Figure 1 shows these heats of adsorption

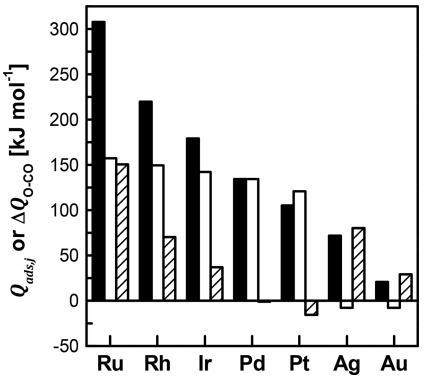

Figure 1. DFT calculated heats of O* (■) and CO* (□) adsorption {$Q_{ads,j}$, where $Q_{ads,j} = -\Delta H_{ads,j}$; j = O* $1/2(O_2 + 2* \rightarrow 2O*)$ or CO* $(CO + * \rightarrow CO*)$}, and their difference ($\Delta Q_{O-CO} = Q_{ads,O} - Q_{ads,CO}$, ⧄) for uncovered Ru(0001),[14,18] Rh(111),[14,18] Ir(111),[13,18] Pd(111),[14,18] Pt(111),[14,18] Ag(111),[14,18] and Au(111) surfaces.[14,18]

$Q_{ads,O}$ and $Q_{ads,CO}$ and their difference (ΔQ_{O-CO}) for uncovered (0001) surfaces of Ru and (111) surfaces of Rh, Ir, Pd, Pt, Ag, and Au.[13,14,18] On Pd and Pt surfaces, the differences between the heats of O* and CO* adsorption (ΔQ_{O-CO}) are −1 and −16 kJ mol^{-1}, respectively.[14,18] These ΔQ_{O-CO} values for Pd and Pt indicate that these surfaces preferentially bind to CO* instead of O* during CO oxidation catalysis, as manifested in the measured rate dependencies, which remain valid over wide CO and O_2 pressure ranges at moderate temperatures. Notably, Pt(100)[19,20] and Pd(110)[21] surfaces become partially covered by O* at very low CO ($(1-2) \times 10^{-5}$ kPa) pressures, on which CO* and O* form their respective adsorbate islands and their relative coverages may oscillate. In contrast, Ru, Rh, and Ir are metals with much larger differences between the heats of O* and CO* adsorption (ΔQ_{O-CO}) of 151, 70, and 37 kJ mol^{-1} on Ru(0001),[14,18] Rh(111),[14,18] and Ir(111),[13,18] respectively. On these metals, CO oxidation occurs on CO* covered surfaces only at the limiting condition of high CO and low O_2 pressures, at which they exhibit identical rate dependencies with Pd and Pt catalysts. At the other extreme of low CO and high O_2 pressures, CO turnover rates on these metals {Ru(0001),[7] Rh(111),[7] and Ir(111)[16]} increase linearly with CO pressures and remain independent of O_2 pressures, because their surfaces become saturated with O* instead of CO. This dynamic shift of the surface coverages and the concomitant shift in the rate dependencies have remained as the topic of interest.

In this study, we probe the turnover rates and rate dependencies for CO oxidation on Ag clusters. Unlike group VIII metals and Au, Ag is an abundant and inexpensive group IB metal with a completely filled d band; it binds much more strongly to O* than CO* with an 80 kJ mol^{-1} difference between the heats of O* and CO* adsorption (ΔQ_{O-CO}) on uncovered (111) surfaces.[14,18] This large and positive ΔQ_{O-CO} value suggests that O* may be able to displace the CO* on Ag surfaces during CO oxidation catalysis. In fact, previous kinetic studies have demonstrated the high reactivity of supported Ag clusters for CO oxidation.[22−26] Additionally, DFT studies have modeled the CO oxidation mechanisms by surface reactions with O*[27−30] or O_2*[27,28,30] on Ag(100),[30] Ag(111),[29] Ag_{55} clusters,[27] and Ag_3 clusters supported on MgO(100) slabs.[28] With these ΔQ_{O-CO} values and previous reports in mind, we investigate how coverage transitions on Ag cluster surfaces may influence the CO oxidation kinetics and reaction mechanisms. We show that the chemical identity of the most abundant surface intermediate (MASI, either O* or CO*) on Ag clusters is a single-valued function of the operating $[O_2]$-to-$[CO]^2$ ratio; thus this ratio is a unique and rigorous descriptor that dictates the operating regime, related rates, and kinetic dependencies. This mechanistic connection relating the operating pressure ratio to the identity of the surface coverages and then to the kinetic dependencies leads the first-order rate coefficients ($r_{CO}[CO]^{-1}$) to depend strictly on the $[O_2]$-to-$[CO]^2$ ratios. There are two distinct kinetic regimes, because the identity of the most abundant surface intermediate changes from CO* to O* in response to an increase in the $[O_2]$-to-$[CO]^2$ ratio. The rate coefficients in these two regimes exhibit different sensitivities to temperature and Ag cluster diameter, as their rate expressions, effective activation barriers, and sensitivities of kinetic parameters differ.

2. CATALYST SYNTHESIS AND EXPERIMENTAL METHODS

2.1. Synthesis of Nanometer Sized Ag, Pd, and Pt Clusters Dispersed on Porous SiO_2 or Al_2O_3 Particles. Supported silver (1−5 wt % Ag/SiO_2), palladium (1 wt %

DOI: 10.1021/acscatal.8b01760
ACS Catal. 2018, 8, 11987−11998

Pd/Al_2O_3), and platinum (1.83 wt % Pt/Al_2O_3) catalysts were prepared by the incipient wetness impregnation method. The CO oxidation activities were insensitive to the identity of the support due to the lack of support contributions to the rate and the structure insensitivity of the reaction rates, as discussed in sections 3.1 and 3.4. Silica (Davisil Chromatographic Silica, 1.2 $cm^3\ g^{-1}$ pore volume, 15 nm pore diameter, 330 $m^2\ g^{-1}$ surface area) and alumina (Sasol, PURALOX TH 100/150, 0.90 $cm^3\ g^{-1}$ pore volume, 11 nm pore diameter, 150 $m^2\ g^{-1}$ surface area) supports were crushed to particle size ranges of 0−75 μm. Silica was heated at 0.033 K s^{-1} in stagnant ambient air to and held at 673 K for 4 h, before cooling to 393 K. Alumina was treated similarly, but to 873 K for 4 h. These treated support particles were impregnated with an aqueous solution of $AgNO_3$ (Sigma-Aldrich, 99.9999% trace metals basis), $Pd(NO_3)_2{\cdot}2H_2O$ (Sigma-Aldrich, 99.995% trace metals basis), or $Pt(NH_3)_4(NO_3)_2$ (Sigma-Aldrich, 99.995% trace metals basis) in doubly deionized water (>18.2 MΩ cm). The impregnated samples were then dried for 24 h at 353 K in stagnant ambient air and then treated in flowing dry air (Linde, 99.99%) at 0.5 $cm^3_{STP}\ g^{-1}\ s^{-1}$ by heating at 0.033 K s^{-1} to 773 K for Ag samples and to 673 K for Pd and Pt samples, followed by holding at these temperatures for 2 h, and then cooling to ambient temperature. The samples were heated at 0.033 K s^{-1} under flowing H_2 (0.5 $cm^3_{STP}\ g^{-1}\ s^{-1}$, Linde certified standard, 5.22% in He) to 598−873 K and then held for 5 h to obtain Ag, Pd, and Pt clusters with mean diameters ranging from 3.1 to 29.3 nm, as summarized in Table 1. The samples were cooled

Table 1. Synthesis Conditions and Mean Cluster Diameters for 1−5 wt % Ag/SiO_2, 1 wt % Pd/Al_2O_3, and 1.83 wt % Pt/Al_2O_3 Catalysts

metal loading	treatment temp in flowing dry air [K]	treatment temp in flowing H_2 [K]	mean cluster diam [nm]
1 wt % Ag	773	598	3.1
5 wt % Ag	773	598	5.1
1 wt % Ag	773	723	11.3
5 wt % Ag	773	723	29.3
1 wt % Pd	673	873	9.3
1.83 wt % Pt	673	873	11.2

in flowing He (0.5 $cm^3_{STP}\ g^{-1}\ s^{-1}$, Linde, 99.999%) to ambient temperature. A mixture of 1% O_2, 4% N_2, and 95% He, prepared from mixing air (Linde, 99.99%) and He (Linde, 99.999%), was introduced to the samples at 0.5 $cm^3_{STP}\ g^{-1}\ s^{-1}$ and ambient temperature for 6 h. Ag/SiO_2, Pd/Al_2O_3, and Pt/Al_2O_3 catalyst powders (0−75 μm particle diameter) were physically mixed with treated silica (SiO_2, Davisil Chromatographic Silica, 1.2 $cm^3\ g^{-1}$ pore volume, 15 nm pore diameter, 330 $m^2\ g^{-1}$ surface area) at silica-to-catalyst mass ratios of 49, 99, and 499. These mixtures were pressed into 2.5 cm diameter pellets at 190 MPa for 0.5 h in a hydraulic press (Specac). The resulting disk was then crushed and sieved to obtain intraparticle diluted catalyst agglomerates with a particle size range of 125−180 μm.

2.2. Isothermal O_2, H_2, and CO Uptake Measurements. O_2, H_2, and CO uptakes were measured at 313−443 K using a volumetric adsorption−desorption apparatus. The apparatus was made of a dosing manifold (10.6 cm^3_{STP}) and reaction chamber (11.4 cm^3_{STP}) connected to a pressure transducer (120AA Baratron, MKS, dual mode 0−13 kPa and 0−133 kPa), six-port valve (H-EHC6WEZ, VICI), vacuum turbopump (Pfeiffer, HiPace 80), and diaphragm pump (Pfeiffer, MVP 015-2). Gases were introduced to the manifold with thermal mass flow controllers (SLA5850, Brooks). Catalyst samples were loaded into a quartz sample holder, heated under flowing H_2 (0.5 $cm^3_{STP}\ g^{-1}\ s^{-1}$, Linde, 99.999%) at 0.033 K s^{-1} to their respective H_2 treatment temperatures used during catalyst synthesis (Table 1) and then held at the temperature for 1 h. The samples were evacuated for at least 12 h at 598−873 K before cooling to 313−443 K at 0.033 K s^{-1} (10^{-5} Pa vacuum, $<5 \times 10^{-8}$ $cm^3_{STP}\ h^{-1}$ leak rate). O_2 and CO uptakes on Ag clusters were measured at 443 K, O_2 uptakes on Pd clusters were measured at 313 K, and H_2 uptakes on Pt clusters were measured at 313 K by introducing doses of 2−16 μmol of O_2 (Linde, 99.995%), H_2 (Linde, 99.999%), or 4.95% CO in He (Linde certified standard) to the sample at 0.08−1 h intervals, which results in incremental pressures of 0.1−1 kPa in the sample holder, up to 13 kPa. Adsorption equilibrium was considered attained when the pressure changes were smaller than 0.01% over a 60 s period. Following the completion of the O_2, CO, or H_2 uptake measurements, the sample was evacuated for an hour at 313−443 K under dynamic vacuum (10^{-5} Pa) before another series of uptake measurements were carried out over the same pressure range. The mean Ag, Pd, and Pt cluster diameters were determined from the difference between the first and second O_2 or H_2 uptakes, extrapolated to zero pressure,[31] assuming an atomic ratio for adsorbate-to-exposed metal of unity ($O_s/Ag_s = O_s/Pd_s = H_s/Pt_s = 1$; subscript "s" denotes surface atom)[31,32] and hemispherical Ag, Pd, and Pt clusters with densities similar to bulk Ag, Pd, and Pt metals (10.49, 12.02, and 21.45 g cm^{-3}, respectively[33]).

2.3. Rate Assessments of CO−O_2 Reactions on Ag, Pd, and Pt Clusters. Rates of CO−O_2 reactions were measured in a fixed bed microcatalytic quartz reactor (8.1 mm i.d.) operating under differential conditions (<1.8% O_2 and <4.1% CO conversion). Intraparticle diluted Ag/SiO_2, Pd/Al_2O_3, and Pt/Al_2O_3 catalyst agglomerates (125−180 μm) were physically mixed with quartz (SiO_2, Sigma-Aldrich, purum p.a., 125−180 μm), which was treated in stagnant ambient air by heating to 673 K for 4 h, at quartz-to-catalyst interparticle dilution mass ratios of 0 (undiluted), 400, and 450. This physical mixture, which contains 0.0002−0.001 g of undiluted Ag/SiO_2, Pd/Al_2O_3, or Pt/Al_2O_3, was loaded into the quartz reactor and formed the packed catalyst bed supported by a quartz frit. The reactor was placed in a furnace (Bluewater Heater) equipped with a K-type thermocouple (Omega) in contact with the catalyst bed. The sample was first pretreated with H_2 (0.333 $cm^3_{STP}\ g^{-1}\ s^{-1}$, Linde, 99.999%) by heating at 0.033 K s^{-1} to 598−873 K, holding for 1 h, and then cooling to the reaction temperature (383−453 K) at 0.033 K s^{-1} in flowing He (0.333 $cm^3_{STP}\ g^{-1}\ s^{-1}$, Linde, 99.999%). Reactant gas mixtures of either 5.5% O_2 in He (Linde certified standard) or O_2 (Linde, 99.999%), 4.95% CO in He (Linde certified standard), and He (Linde, 99.999%) were introduced by independently metering the individual flow rates using thermal mass flow controllers (SLA5850, Brooks). The CO−O_2 reaction rates were measured in the kinetically controlled regime upon reaching steady state (>4 h), at which the CO turnover rates are independent of time at a set of reference conditions {0.25 kPa O_2, 0.2 kPa CO, $(0.08-2) \times 10^8$ cm^3_{STP} (g-atom of M_s $s)^{-1}$, where M is Ag, Pt, or Pd}. The changes in catalytic rates with time were found to be less than 4% on average when measured at the reference conditions after the entire duration of rate measurements (<16 h). The chemical compositions of the reactor effluent were quantified at 0.05 h intervals with a gas chromatograph (8610C, SRI) equipped with a molecular sieve 13X (6 ft × 1/8 in. SS, SRI) packed column,

DOI: 10.1021/acscatal.8b01760
ACS Catal. 2018, 8, 11987−11998

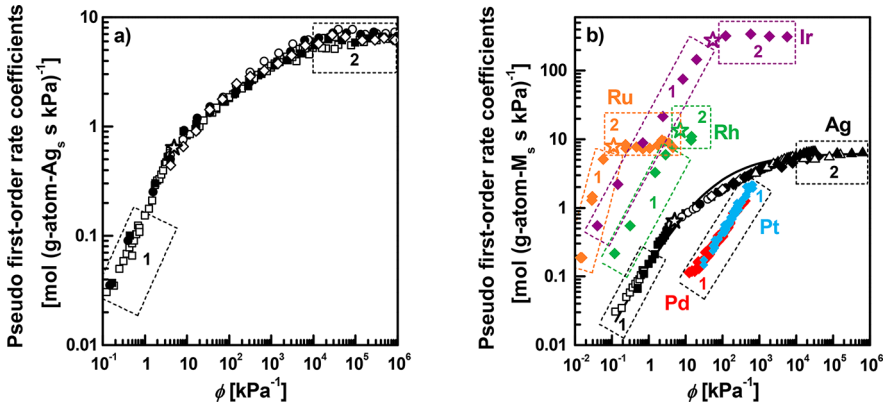

Figure 2. (a) Pseudo-first-order rate coefficients ($k^{1st} = r_{CO}[CO]^{-1}$, eq 2a) for CO−$O_2$ reactions at 443 K as a function of ϕ ($[O_2][CO]^{-2}$) on 5.1 nm Ag clusters (5 wt % Ag/SiO_2) diluted at silica-to-Ag/SiO_2 intraparticle dilution mass ratios of 49 (○, ●), 99 (□, ■), and 499 (◇), as well as quartz-to-Ag/SiO_2 interparticle dilution mass ratios of 0 (undiluted) (○, □, ◇), 400 (■), and 450 (●) (total SiO_2-to-Ag/SiO_2 dilution mass ratio is 499, (0.5−2) × 10^8 cm^3_{STP} (g-atom of Ag_s)$^{-1}$ s^{-1}). (b) Pseudo-first-order rate coefficients as a function of ϕ from data taken from the literature for Ru(0001)[7] (orange ◆, 500 K, 2.1 kPa CO), Rh(111)[7] (green ◆, 500 K, 2.1 kPa CO), and Ir(111)[16] (purple ◆, 525 K, 2.7 kPa CO), as well as our work for 9.3 nm Pd clusters (red ◆, Pd/Al_2O_3, 400 K, 0.5−1 kPa O_2, 0.05−0.2 kPa CO), 11.2 nm Pt clusters (blue ◆, Pt/Al_2O_3, 453 K, 5−70 kPa O_2, 0.15−0.8 kPa CO), and 5.1 nm Ag clusters {443 K; 0.0125 (▲), 0.025 (△), 0.05 (◆), 0.1 (◇), 0.2 (●), 0.5 (○), 1 (■), and 2 (□) kPa CO}, and calculated rate coefficients for 5.1 nm Ag clusters using eq 6b and regressed parameters from Table 2 (—). Labels 1, 2, and ☆ indicate regimes 1, 2, and the midpoint of the transition between them (ϕ_t, eqs 11 and 12), respectively.

connected to a thermal conductivity detector (TCD) and then a micromethanizer and flame ionization detector (FID).

3. RESULTS AND DISCUSSION

3.1. Metal Identity Effects on Rate Dependencies during CO Oxidation Reactions. CO−O_2 reactions turn over on transition metals much faster than other reactions at low to moderate temperatures. The larger rates, taken together with the significant reaction exothermicity {CO + 0.5O_2 → CO_2, ΔH_r° = −284 kJ (mol of CO)$^{-1}$}, may lead to temperature and concentration gradients that corrupt the accurate assessments of intrinsic rates. In this study, we decrease the reactor heat load (heat generated per unit reactor volume) by diluting the catalyst powders extensively with inert solids within the particles and in the catalyst packed bed. Such dilutions remove temperature and concentration gradients. The first-order rate coefficient in CO pressures (k^{1st}) equals the CO turnover rate (per exposed Ag site, r_{CO}) divided by CO pressure [CO], whereas ϕ is the operating pressure ratio of O_2 to the square of CO:

$$k^{1st} = \frac{r_{CO}}{[CO]} \tag{2a}$$

$$\phi = \frac{[O_2]}{[CO]^2} \tag{2b}$$

Figure 2a reports the rate coefficients (k^{1st}) on a series of 5 wt % Ag/SiO_2 catalysts (5.1 nm average Ag cluster diameter) with different dilution extents over a wide range of ϕ values between 0.13 and 10^6 kPa^{-1} at 443 K. For one series of samples, the intraparticle silica-to-Ag/SiO_2 catalyst dilution mass ratio was varied from 49, 99, and 499 with no interparticle dilution. For the other sample series, the interparticle quartz-to-Ag/SiO_2 catalyst dilution mass ratio was varied from 0, 400, and 450, during which the intraparticle dilution mass ratio was changed commensurately, such that the total SiO_2, which includes both the quartz and the SiO_2 diluents, to Ag/SiO_2 catalyst mass ratio was kept constant at 499. Among all these cases of different dilution levels, the first-order rate coefficients were nearly identical (<10% difference) when comparing at the same ϕ value, thus confirming that the dilution level used in our rate measurements did not influence the turnover rate values. The maximum heat loads from the rate data reported herein with these dilution ratios (0.72 W $cm^{-3}_{reactor\ bed}$) are similar to those with similar reactor configurations (8.1 mm i.d. quartz reactor, 423−773 K), previously shown to be free of transport corruptions during CO oxidation kinetic studies.[10,11] In addition, CO oxidation rate ratios on bare SiO_2 to those on 5 wt % Ag/SiO_2, $r_{SiO_2} r_{Ag/SiO_2}^{-1}$ (comparing at the same mass basis), are less than 0.04 under all operating conditions reported herein (0.25−100 kPa O_2, 0.0125−2 kPa CO, 383−443 K). Thus, rate contributions from SiO_2 are insignificant (<4%). We conclude, based on these assessments, that a packed catalyst bed with an intraparticle dilution mass ratio greater than 49 and an interparticle dilution mass ratio of 0 is sufficient in eliminating all concentration and temperature gradients. Furthermore, identical intra- and interparticle dilution mass ratios are sufficient to remove these gradients on Pd/Al_2O_3 and Pt/Al_2O_3 catalysts, due to their lower reactivity and heat loads than Ag/SiO_2 catalysts, as well as low contributions from Al_2O_3 (<5%). Thus, CO conversion rates measured with this packed catalyst bed must reflect the intrinsic reactivities of Ag, Pd, and Pt clusters, free of transport corruptions and support effects.

Figure 2 shows the first-order rate coefficients (k^{1st}, eq 2a) on Ag clusters (5.1 nm mean diameter, 5 wt % Ag/SiO_2) at 443 K over a wide range of O_2 (0.25−100 kPa) and CO (0.0125−2 kPa) pressures, plotted as a function of ϕ (eq 2b). We did not observe oscillatory kinetic behaviors previously attributed to surface reconstructions and adsorbate island formations on Pt(100)[19,20] and Pd(110)[21] surfaces, indicating that Ag cluster surfaces can be described as Langmuirian surfaces. We report reaction rates obtained at atmospheric pressures, where CO* and O* coverages are always near saturation, instead of those obtained with surface science studies under high vacuum conditions and at much lower coverages, at which CO* and O* can form their respective adsorbate islands on Pd and Pt surfaces.[19−21] These rate coefficients are single-valued functions of the ϕ values and exhibit two distinct dependencies,

DOI: 10.1021/acscatal.8b01760
ACS Catal. 2018, 8, 11987−11998

irrespective of the individual O_2 or CO pressures. We denote the two distinct dependencies as regimes 1 and 2, defined by the operating ϕ values from 0.13 to 1 kPa^{-1} and from 10^4 to 6.4×10^5 kPa^{-1}, respectively, as also indicated in Figure 2. First-order rate coefficients in regime 1 (ϕ = 0.13−1 kPa^{-1}), k_1^{1st}, increase linearly with ϕ (eq 3a), because the CO turnover rates, $r_{CO,1}$, increase linearly with O_2 pressure and with the inverse of CO pressure, as captured by eq 3b and shown in Figure S1 of the Supporting Information:

regime 1:

$$k_1^{1^{st}} = k_{eff,1}\left(\frac{[O_2]}{[CO]^2}\right) = k_{eff,1}\phi^1 \tag{3a}$$

regime 1:

$$r_{CO,1} = k_{eff,1}\frac{[O_2]}{[CO]} = k_{eff,1}\phi^1[CO] \tag{3b}$$

where $k_{eff,1}$ denotes the effective rate constant for regime 1. In contrast, first-order rate coefficients in regime 2 ($\phi = 10^4$−6.4×10^5 kPa^{-1}), k_2^{1st}, are independent of the ϕ values and remain a true constant at 7 mol (g-atom of Ag_s s $kPa)^{-1}$ at 443 K (eq 4a), because the CO turnover rates in regime 2, $r_{CO,2}$, are insensitive to O_2 pressure and increase linearly with CO pressure, as shown also in Figure S1 of the Supporting Information:

regime 2:

$$k_2^{1^{st}} = k_{eff,2}\phi^0 \tag{4a}$$

regime 2:

$$r_{CO,2} = k_{eff,2}[CO] = k_{eff,2}\phi^0[CO] \tag{4b}$$

where $k_{eff,2}$ denotes the effective rate constant for regime 2.

At moderate temperatures (400−525 K), CO turnover rates on group VIII transition metals (Ru, Rh, Ir, Pd, Pt) may exhibit rate dependencies in either regime 1 or regime 2, depending on the operating ϕ value, as shown in Figure 2b. On Pd (9.3 nm, 400 K) and Pt (11.2 nm, 453 K) clusters, CO oxidation shows the characteristic rate dependencies of regime 1 (eqs 3a and 3b) over the entire operating range of ϕ values (13−667 kPa^{-1}). Others have also observed similar kinetic manifestations {Pd(100),[8] Pd(110),[16] Pd(111),[9] Pt(100),[16] and 1.2−20 nm Pt clusters[10]} for a wide range of ϕ values ($(0.02-1.7) \times 10^3$ kPa^{-1}). Other metals such as Ag, Ru, Rh, and Ir also exhibit these rate dependencies typical for regime 1, but only limited to much smaller ϕ ranges, from 0.13 to 1 kPa^{-1} on Ag clusters (5.1 nm, 443 K), from 5×10^{-3} to 0.03 kPa^{-1} on Ru(0001) at 500 K,[7] from 0.02 to 6 kPa^{-1} on Rh(111) at 500 K,[7] and from 4×10^{-2} to 10 kPa^{-1} on Ir(111) at 525 K,[16] as included in Figure 2b. Similar to those on 5.1 nm Ag clusters (Figure 2), CO rate dependencies on Ru(0001),[7] Rh(111),[7] and Ir(111)[16] surfaces undergo a transition from regime 1 to regime 2, as the operating ϕ values increase. For example, the rate dependencies on Ru(0001) surfaces at 500 K resemble those in regime 1 for ϕ values between 0.01 and 0.06, but change to those in regime 2, as the operating ϕ values increase to above 0.1.[7] Auger electron spectroscopy (AES) measurements on the Ru(0001) sample carried out after steady-state reactions at various ϕ values show that the O* coverages vary commensurately from essentially uncovered in regime 1 to near saturation in regime 2.[7] The transition in kinetic dependencies between the two distinct regimes (regimes 1 and 2), reported here for Ag clusters and detected previously for Rh, Ru, and Ir surfaces, albeit without a mechanistic description, suggests a dynamic shift in the identity of most abundant surface intermediates from CO* in regime 1 to O* in regime 2.

The kinetic transition between regimes 1 and 2 occurs at different ϕ values on Ag clusters (5.1 nm), Ru(0001),[7] Rh(111),[7] and Ir(111).[16] The transition, labeled in Figure 2 as ϕ_t, occurs at the lowest ϕ value of 0.07 kPa^{-1} on Ru(0001) at 500 K,[7] followed by 4 kPa^{-1} on Ag clusters at 443 K, 6 kPa^{-1} on Rh(111) at 500 K,[7] and 50 kPa^{-1} on Ir(111) at 525 K.[16] The kinetic transition on these metals appears to correlate with the difference in their heats of O* and CO* adsorption (ΔQ_{O-CO}, eq 1), in the decreasing order of Ru, Ag, Rh, and Ir (151 kJ mol^{-1} > 80 kJ mol^{-1} > 70 kJ mol^{-1} > 37 kJ mol^{-1}, respectively, Figure 1). Metals with smaller and negative ΔQ_{O-CO} values such as Pd and Pt (Figure 1) only exhibit rate dependencies characteristic of regime 1. Although Ag binds to both O* and CO* much more weakly than other transition metals, it has a higher ΔQ_{O-CO} value among all metals except for Ru and thus binds to O* much more strongly than CO*. For this reason, Ag cluster surfaces remain preferentially covered with O* rather than CO* during CO oxidation catalysis, previously unattainable at the moderate temperatures on Pd and Pt clusters. On such O* covered surfaces, CO* no longer inhibits CO oxidation; thus all sites may be able to participate in catalytic turnovers.

Since the CO turnover rates are functions of the operating CO and O_2 pressures (eqs 3b, 4b), we extract and summarize the effective rate coefficients in regimes 1 ($k_{eff,1}$) and 2 ($k_{eff,2}$) such that we could directly compare their values among Ag, Pd, and Pt clusters (this work: 5.1 nm Ag, 9.3 nm Pd, 11.2 nm Pt; literature: 1.2−20 nm Pt[10]) and on Pt(100),[16] Pd {(100),[8] (110),[16] (111)[9]}, Rh(111),[7] Ir(111),[16] and Ru(0001)[7] surfaces. Figure 3a shows the effective rate coefficients for the different metals in regime 1. In this regime, the effective rate coefficients on all metals except Pt are within 1 order of magnitude from each other over the temperature range 373−600 K, and their values are 2 orders of magnitude larger than those of Pt. Similarly, Figure 3b compares the effective rate coefficients of regime 2 for Ru, Rh, Ir, and Ag supported catalysts and single crystals. In this regime, the effective rate coefficients on 5.1 nm Ag clusters are 1−2 orders of magnitude larger than those on Ru(0001). Furthermore, the extrapolated rate coefficients on 5.1 nm Ag clusters (from 383 to 443 K) are within 1 order of magnitude from those of Rh(111) (500 K) and Ir(111) (525 K). These results in Figure 3 indicate that Ag clusters (1) exhibit similar reactivities to group VIII transition metals for CO oxidation while operating in regime 1, during which metal surfaces remain covered with CO* inhibitors, and (2) remain more reactive than group VIII transition metals in regime 2, when metal surfaces are free of CO* and covered with O*. We note that small Au clusters appear to catalyze $CO-O_2$ reactions at much lower temperatures than group VIII transition metals and Ag; e.g., the CO oxidation turnover rates on 2.8−3.5 nm Au clusters[5,34] at 288−300 K are within an order of magnitude {0.05−0.5 mol (g-atom of $M_s)^{-1}$, where M_s denotes surface metal atoms} of those on 9.3 nm Pd, 11.2 nm Pt, and 5.1 nm Ag clusters at 373−461 K and similar reactant pressure ranges (10^{-1} kPa^{-1} < ϕ < 10^4 kPa^{-1}). On Au catalysts, the reaction orders toward O_2 and CO are between zero and one,[17,35] suggesting that Au cluster surfaces are partially covered by O*, CO*, or both, likely due to the small heats of

DOI: 10.1021/acscatal.8b01760
ACS Catal. 2018, 8, 11987−11998

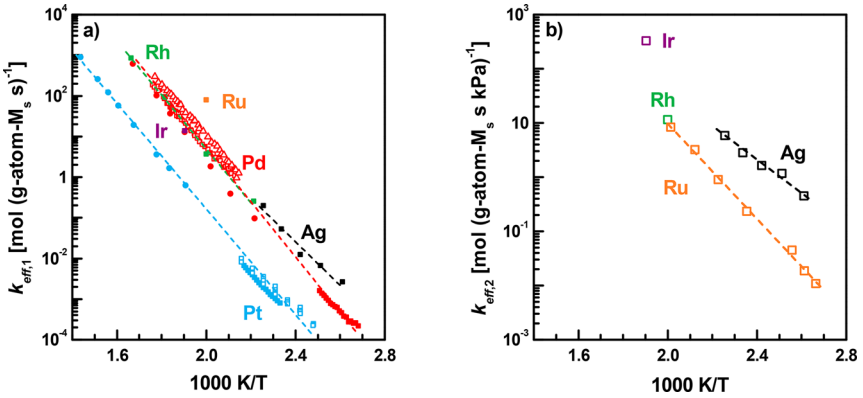

Figure 3. (a) CO oxidation effective rate constants for regime 1 ($k_{eff,1}$, eqs 3a and 3b) as a function of inverse temperature for CO−O_2 reactions from data taken from the literature for Ru(0001)[7] (orange ■, ϕ = 0.005−0.02 kPa^{-1}), Rh(111)[7] (green ■, ϕ = 0.1−6 kPa^{-1}), Ir(111)[16] (purple ■, ϕ = 0.04−10 kPa^{-1}), Pd(100)[8] (red △, ϕ = 3.8 kPa^{-1}), Pd(110)[16] (red ●, ϕ = 0.23 kPa^{-1}), Pd(111)[9] (red □, ϕ = 3.8 kPa^{-1}), Pt(100)[16] (blue ●, ϕ = 0.23), and 1.2−20 nm Pt clusters[10] (blue □, ϕ = 10^3 kPa^{-1}), as well as our work for 9.3 nm Pd clusters (red ■, ϕ = 10^3 kPa^{-1}), 11.2 nm Pt clusters (blue ■, ϕ = 3.8 × 10^2 kPa^{-1}), and 5.1 nm Ag clusters (■, ϕ = 0.13−1 kPa^{-1}, Table 2). (b) CO oxidation effective rate constants for regime 2 ($k_{eff,2}$, eqs 4a and 4b) as a function of inverse temperature for CO−O_2 reactions from data taken from the literature for Ru(0001)[7] (orange □, ϕ = 0.23 kPa^{-1}), Rh(111)[7] (green □, ϕ = 7−14 kPa^{-1}), and Ir(111)[16] (purple □, ϕ = 10^2−6 × 10^3 kPa^{-1}), as well as our work for 5.1 nm Ag clusters (□, ϕ = 10^4−6.4 × 10^5 kPa^{-1}, Table 2).

Scheme 1. Proposed Sequence of Elementary Reactions for CO Oxidation Reactions on Ag Clusters[a]

Step	Elementary Reaction	Rate or Equilibrium Constant
1	$O_2 + * \rightleftarrows O_2*$	K_{O_2}
2	$O_2* + * \rightleftarrows 2O*$	k_{O_f}, k_{O_r}, K_O
3	$CO + * \rightleftarrows CO*$	K_{CO}
4 (Pathway A)	$CO* + O_2* \not\rightarrow CO_2 + O* + *$	$k_{CO\text{-}O_2}$
5 (Pathway B)	$CO* + O* \not\rightarrow CO_2 + * + *$	$k_{CO\text{-}O}$

[a] * denotes an active site, → with ∧ through it denotes an irreversible step, ⇄ denotes a reversible step, and ⇄ with a circle through it denotes a quasi-equilibrated step. K_j is the equilibrium constant, k_j or k_{jf} is the forward rate constant, and k_{jr} is the reverse rate constant for step j.

adsorption of O* and CO* on Au, relative to the group VIII transition metals and Ag.

3.2. Elementary Steps and Rate Expressions for CO−O_2 Reactions on Dispersed Ag Clusters. Scheme 1 shows a proposed sequence of elementary steps for CO oxidation on Ag clusters that captures the observed dependencies for the rate coefficients k_1^{1st} and k_2^{1st} and turnover rates $r_{CO,1}$ and $r_{CO,2}$ for both regimes, as shown in Figure 2b and Figure S1, over the entire operating ϕ values ((0.13−6.4) × 10^5 kPa^{-1}). The reaction begins with quasi-equilibrated molecular O_2 adsorption on a vacant Ag site (*) as O_2* (step 1), followed by reversible O_2* dissociation that forms two O* adatoms (step 2). CO adsorbs on a vacant site in a quasi-equilibrated step (step 3) as CO*, followed by its irreversible reaction with either a molecular O_2* (step 4, pathway A) or an O* adatom (step 5, pathway B), forming CO_2 and O* or only CO_2, respectively. These reactions complete the catalytic cycle. Both pathways A and B are plausible and have been previously proposed to occur on Ag[27−30] and Pt.[10,11] Both the O_2* dissociation (forward reaction of step 2) and CO* reaction with O_2* (step 4) generate O* atoms, whereas the O* recombination (reverse reaction of step 2) and the CO* reaction with O* (step 5) consume O* atoms.

We derive, from the elementary reactions proposed in Scheme 1, the general form of the governing rate equation for CO oxidation via pathways A and B that results in the apparent rate dependencies in regimes 1 and 2 (eqs 3a,3b, 4a, and 4b, full derivation in section S2 of the Supporting Information):

$$r_{CO} = r_{CO,\text{Pathway A}} + r_{CO,\text{Pathway B}}$$

$$r_{CO} = \frac{k_{CO\text{-}O_2} K_{O_2} K_{CO} [CO][O_2] + \frac{(k_{CO\text{-}O} K_{CO}[CO])^2}{4k_{O_r}} \left[\sqrt{1 + \frac{8k_{O_f} K_{O_2}}{(k_{CO\text{-}O} K_{CO})^2} \frac{[O_2]}{[CO]^2} \left(2k_{O_f} + k_{CO\text{-}O_2} K_{CO}[CO]\right)} - 1\right]}{\left(1 + \frac{k_{CO\text{-}O} K_{CO}[CO]}{4k_{O_r}} \left[\sqrt{1 + \frac{8K_{O_2} k_{O_r}}{(k_{CO\text{-}O} K_{CO})^2} \frac{[O_2]}{[CO]^2} \left(2k_{O_f} + k_{CO\text{-}O_2} K_{CO}[CO]\right)} - 1\right] + K_{O_2}[O_2] + K_{CO}[CO]\right)^2} \quad (5)$$

(↑ * ; ↑ O* ; ↑ O_2* ; ↑ CO*)

where k_{CO-O_2} and k_{CO-O} are the rate constants for CO* reactions with O_2* via pathway A and with O* via pathway B, respectively; K_{O_2} and K_{CO} are the equilibrium constants for O_2* and CO* adsorption, respectively; k_{O_f} and k_{O_r} are the forward and reverse rate constants for O_2* dissociation, respectively. These rate and equilibrium constants are defined in Scheme 1.

Nonlinear regression of eq 5 against the rate data in Figure 2b provides the rate parameter values for CO−O_2 reactions on 5.1 nm Ag clusters at 443 K, as summarized in Table S1 of the Supporting Information. These parameters, together with eqs S8−S13 in section S2 of the Supporting Information, determine the relative rate contributions of pathways A and B, as well as the relative surface coverages of O*, O_2*, and CO*

DOI: 10.1021/acscatal.8b01760
ACS Catal. 2018, 8, 11987−11998

Table 2. Rate and Equilibrium Constants for CO Oxidation Reactions on 5 wt % Ag/SiO_2 (5.1 nm Ag clusters) at 383−443 K from Nonlinear Regression of CO−O_2 Reaction Rate Data (Figures 2a and 7) against the Proposed Rate Expression (eq 6b)

temp [K]	$k_{eff,1}$ [a] [mol (g-atom of Ag_s s)$^{-1}$]	$k_{eff,2}$ [b] [mol (g-atom of Ag_s s kPa)$^{-1}$]	K_{O-CO} [c] [kPa$^{-0.5}$]
443	0.20 ± 0.01	6.1 ± 0.3	0.18 ± 0.01
428	0.052 ± 0.008	2.8 ± 0.4	0.14 ± 0.02
413	0.012 ± 0.002	1.6 ± 0.2	0.087 ± 0.012
398	0.0070 ± 0.0015	1.2 ± 0.1	0.074 ± 0.011
383	0.0030 ± 0.0007	0.5 ± 0.1	0.080 ± 0.012

[a] $k_{eff,1} = \frac{k_{CO-O_2}K_{O_2}}{K_{CO}}$ in eq 7. [b] $k_{eff,2} = \frac{k_{CO-O_2}K_{CO}}{K_O}$ in eq 8. [c] $K_{O-CO} = \frac{K_{O_2}^{0.5}K_O^{0.5}}{K_{CO}}$ in eq 9.

intermediates, as summarized in Table S2. From the rate contributions, we conclude that pathway B (step 5) contributes to less than 5% of the total CO turnovers under most reaction conditions [$r_{CO,pathway\ B}(r_{CO,pathway\ A} + r_{CO,pathway\ B})^{-1} < 0.05$ for $\phi = (2-6.4) \times 10^5$ kPa^{-1}]. At the smallest ϕ value (0.13), pathway B contributes to at most 13% of the total CO turnover rate. The regressed parameters in Table S1 also imply the reversibility of O_2 dissociation, which relates to the relative rate ratios of the competitive O_2* dissociation, O* recombination, CO*−O_2*, and CO*−O* reactions. Since the rate of pathway B is negligible, O_2 recombination (the reverse of step 2) removes O* adatoms much more rapidly than CO*−O* reactions (step 5). Furthermore, the values in Table S1 reveal that O_2 dissociation (step 2) generates O* adatoms much faster than CO*−O_2* reactions (step 4) ($2k_{O_f} \gg k_{CO-O_2}K_{CO}[CO]$). Over the entire range of reactant pressures and reaction temperatures, the rates of O_2 dissociation and O* recombination are nearly equal to each other (<16% different) and their magnitudes are at least 1 and up to 4 orders of magnitude larger than the CO−O_2* and CO−O* reaction rates. These results suggest that the O_2 dissociative step (step 2) is quasi-equilibrated. Finally, the fractions of vacant Ag sites (*) and sites occupied by O_2* remain below 0.02 and 0.005 ML, respectively, under all reaction conditions. In addition, sensitivity analyses show that k_{CO-O} and K_{O_2} are insensitive to the perturbation of their values: a 20% variation in their magnitude increases the residual sum of squared errors by 20 ± 17% (Figure S2).

Based on the above interpretations, we conclude that the rate of the CO*−O* reaction ($r_{CO,pathway\ B}$) remains kinetically insignificant, the O_2 dissociation step is quasi-equilibrated, and the fractions of uncovered Ag sites (∗) and adsorbed O_2* are small. Taken together, these approximations result in the simplified equations for turnover rate r_{CO} and rate coefficient k^{1st}, considering that the CO_2*−O_2* reaction (pathway A) as the predominant path, taking place on Ag clusters covered with either CO* or O*:

$$r_{CO} = r_{CO,\ Pathway\ A} = \frac{k_{CO\text{-}O_2}K_{O_2}K_{CO}[CO][O_2]}{\left(K_{O_2}^{0.5}K_O^{0.5}\sqrt{[O_2]} + K_{CO}[CO]\right)^2} \quad \begin{matrix} \uparrow & \uparrow \\ O^* & CO^* \end{matrix} \tag{6a}$$

$$k^{1st} = \frac{r_{CO}}{[CO]} = \frac{\frac{k_{CO\text{-}O_2}K_{O_2}}{K_{CO}}\phi}{\left(\frac{K_{O_2}^{0.5}K_O^{0.5}}{K_{CO}}\sqrt{\phi} + 1\right)^2} \quad \begin{matrix} \uparrow & \uparrow \\ O^* & CO^* \end{matrix} \tag{6b}$$

where K_O is the equilibrium constant for O_2* dissociation ($K_O = k_{O_f}k_{O_r}^{-1}$).

The relative magnitudes of the rate and equilibrium parameters in eqs 6a and 6b, together with the operating conditions, determine the apparent kinetic dependencies of CO−O_2 reaction. In regime 1, when CO* is the most abundant surface intermediate (MASI), the $K_{CO}[CO]$ term in the denominator is much larger than the $K_{O_2}^{0.5}K_O^{0.5}\sqrt{[O_2]}$ term ($K_{CO}[CO] \gg K_{O_2}^{0.5}K_O^{0.5}\sqrt{[O_2]}$). As a result, eqs 6a and 6b simplify to eqs 3a and 3b, the observed rate dependencies for this regime (Figure 2b). The effective rate constant for regime 1 is

regime 1:

$$k_{eff,1} = \frac{k_{CO-O_2}K_{O_2}}{K_{CO}} \tag{7}$$

For the contrasting case of regime 2, when O* instead of CO* is the MASI, $K_{O_2}^{0.5}K_O^{0.5}\sqrt{[O_2]}$ is much larger than $K_{CO}[CO]$ ($K_{O_2}^{0.5}K_O^{0.5}\sqrt{[O_2]} \gg K_{CO}[CO]$) and eqs 6a and 6b reduce to eqs 4a and 4b, which describe the rate dependencies for this regime (Figure 2b). The effective rate constant is

regime 2:

$$k_{eff,2} = \frac{k_{CO-O_2}K_{CO}}{K_O} \tag{8}$$

These two effective rate coefficients, $k_{eff,1}$ and $k_{eff,2}$, fully describe the reactivity dependencies on ϕ for both regimes 1 and 2 in Figure 2b. Specifically, $k_{eff,1}$ is the slope for the rate coefficients at low ϕ values (eq 3a) and $k_{eff,2}$ equals the maximum first-order rate coefficients, which remain constant, at high ϕ values (eq 4a). Since eqs 6a and 6b capture the dependencies for both regimes 1 and 2, k^{1st} becomes a single-valued function of ϕ. Finally, the square root of the $k_{eff,1}$-to-$k_{eff,2}$ ratio, defined as K_{O-CO}, equals the grouping of equilibrium coefficients in eq 6b ($K_{O_2}^{0.5}K_O^{0.5}K_{CO}^{-1}$) and relates to the transition between regimes 1 and 2:

$$K_{O-CO} = \sqrt{\frac{k_{eff,1}}{k_{eff,2}}} = \frac{K_{O_2}^{0.5}K_O^{0.5}}{K_{CO}} \tag{9}$$

Table 2 shows the values for the kinetic ($k_{eff,1}$ and $k_{eff,2}$, eqs 7 and 8) and thermodynamic (K_{O-CO}, eq 9) groupings, determined from the parameters in Table S1. These kinetic and thermodynamic values give the predicted first-order rate coefficients via eq 6b, included in Figure 2b for a direct comparison with the measured values. Figure 4 shows the parity plot comparing the measured (Figure S1) and calculated (from eq 6a and Table 2) rates, showing that the model captures the measured rates. Section S3 in the Supporting Information includes the sensitivity analyses of the estimated parameter values, which indicate that $k_{eff,1}$ and K_{O-CO} are

DOI: 10.1021/acscatal.8b01760
ACS Catal. 2018, 8, 11987−11998

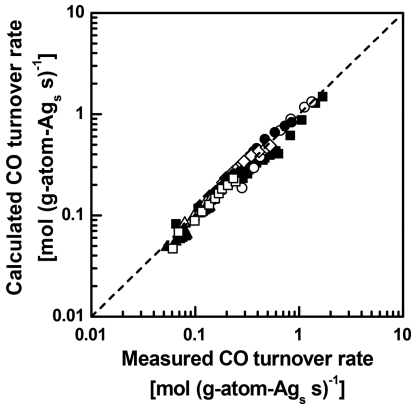

Figure 4. Parity plot between predicted and measured CO turnover rates (per exposed Ag atom, 5 wt % Ag/SiO_2, 5.1 nm clusters) at 443 K. Predicted rates were calculated from eq 6a and regressed kinetic and thermodynamic parameters from Table 2; measured rates were obtained at 0.25−100 kPa O_2 and 0.0125 (▲), 0.025 (△), 0.05 (◆), 0.1 (◇), 0.2 (●), 0.5 (○), 1 (■), and 2 (□) kPa CO ((0.5−2) × 10^8 cm^3_{STP} (g-atom of Ag_s)$^{-1}$ s^{-1}, Figure S1 of the Supporting Information).

highly sensitive to variations of their values: a 20% change in their magnitude increases the residual sum of squared errors by 91 ± 47%.

3.3. CO* and O* Coverages on Ag Cluster Surfaces at Chemical Equilibrium and during Steady-State CO−O_2 Reactions and Their Catalytic Effects That Cause the Transition between the Kinetic Regimes. Isothermal CO uptakes at CO pressures and a temperature similar to those used for steady-state CO oxidation studies (0.01−1.3 kPa CO, 443 K) lead to CO* coverages of up to 0.40 ML on Ag clusters (5.1 nm), as shown in Figure S4a. These uptake data translate to a CO* adsorption equilibrium constant (K_{CO}) of 0.30 kPa^{-1}. By assuming a loss of one translational and one rotational degree of freedom during CO adsorption,[36] which corresponds to an entropy loss ($\Delta S_{ads,CO}$) of −90 J (mol K)$^{-1}$, the average heat of CO* adsorption ($Q_{ads,CO}$) is 53 ± 1 kJ mol^{-1}. This heat of CO adsorption (53 ± 1 kJ mol^{-1}) is larger than the previously reported values on uncovered Ag(111) surfaces of 27 and −8 kJ mol^{-1}, derived based on equilibrium CO uptakes[37] and DFT calculations,[14] respectively. The larger heat of adsorption from the clusters than surfaces is expected, because clusters contain corner and edge sites that bind to CO much more strongly than the terrace sites on Ag(111) surfaces, as predicted from the bond-order conservation principle.[38]

Isothermal, equilibrium O_2 uptakes on 5.1 nm Ag clusters at the same temperature (443 K) and between 0.01 and 13 kPa O_2 (Figure S4b) give the equilibrium constant for dissociative O_2 adsorption, $K_{O_2}K_O$. The $K_{O_2}K_O$ value is 26 kPa^{-1}, which corresponds to an average heat of O* adsorption ($Q_{ads,O}$) of 55 ± 1 kJ (mol of O)$^{-1}$ for Ag clusters with O* coverages ranging from 0.16 to 0.99 ML, assuming that O_2 loses all translational and rotational degrees of freedom during its dissociative adsorption,[39] which is equivalent to an adsorption entropy loss ($\Delta S_{ads,2O*}$, per two O* adatoms) of −181 J (mol of O_2 K)$^{-1}$. This average heat of O* adsorption is similar to those measured on polycrystalline Ag {33−52 kJ (mol of O)$^{-1}$ at 0.68−0.82 ML O*}.[40,41]

During steady-state reactions, both CO* and O* intermediates occupy Ag sites. The instantaneous CO* and O* fractional coverages during steady-state catalysis, denoted as $[CO^*]/[Ag_s]_{SS}$ and $[O^*]/[Ag_s]_{SS}$ (subscript SS denotes steady state), respectively, are:

$$\left(\frac{[CO^*]}{[Ag_s]}\right)_{SS} = \frac{1}{K_{O-CO}\sqrt{\phi} + 1} \quad (10a)$$

$$\left(\frac{[O^*]}{[Ag_s]}\right)_{SS} = \frac{K_{O-CO}\sqrt{\phi}}{K_{O-CO}\sqrt{\phi} + 1} \quad (10b)$$

as derived from the denominator terms of eqs 6a and 6b. As shown in the expressions, these instantaneous CO* and O* coverages are also single-valued functions of ϕ. Equations 10a and 10b, together with the parameters in Table 2, give the CO* and O* coverages during steady-state CO−O_2 reactions shown in Figure 5. In regime 1 (ϕ = 0.13−1 kPa^{-1}), the CO* coverages are larger than 0.85 and O* coverages are smaller than 0.15. In the contrasting case of regime 2 (ϕ = 10^4−6.4 × 10^5 kPa^{-1}), the CO* coverages remain below 0.05; thus O* adatoms occupy almost all Ag sites.

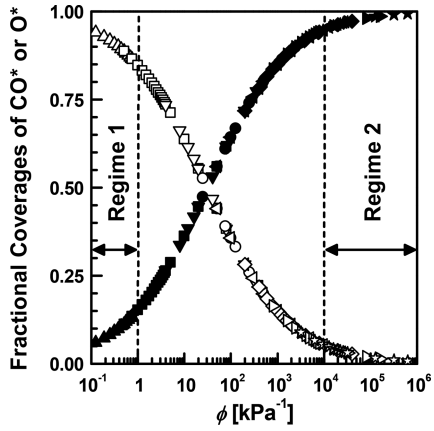

Figure 5. Steady-state fractional coverages of CO* (eq 10a, △, □, ▽, ○, ◁, ◇, ▷, ☆) and O* (eq 10b, ▲, ■, ▼, ●, ◀, ◆, ▶, ★) during CO−O_2 reactions on Ag clusters (5 wt % Ag/SiO_2, 5.1 nm clusters) as a function of ϕ ($[O_2][CO]^{-2}$) at 0.25−100 kPa O_2 and 2 (△, ▲), 1 (□, ■), 0.5 (▽, ▼), 0.2 (○, ●), 0.1 (◁, ◀), 0.05 (◇, ◆), 0.025 (▷, ▶), and 0.0125 (☆, ★) kPa CO at 443 K ((0.5−2) × 10^8 cm^3_{STP} (g-atom of Ag_s)$^{-1}$ s^{-1}).

The equilibrium constant ratio (K_{O-CO}) determined from the rate data regression (0.18 ± 0.01 $kPa^{-0.5}$, Table 2) at 443 K on Ag cluster surfaces nearly saturated with both CO* and O* is much smaller than the value derived from the individual O* and CO* equilibrium uptakes at 443 K $\{(K_{O_2}{}^{0.5}K_O{}^{0.5}K_{CO}{}^{-1})_{equilibrium} = 16 \pm 1\ kPa^{-0.5}\}$, measured independently and without the presence of competing coadsorbates. The much smaller K_{O-CO} value during steady-state reactions, when both reactants are present, than the calculated value derived from individual reactants indicates that interactions between CO* and O* adsorbates at near saturation with a combined coverage approaching 1 ML, which occurs during CO−O_2 reactions, decrease the $K_{O_2}{}^{0.5}K_O{}^{0.5}$-to-$K_{CO}$ ratio relative to those with single adsorbates of either CO* (0−0.40 ML) or O* (0.16−0.99 ML) in CO or O_2 uptakes.

The transition between regimes 1 and 2 occurs gradually over a wide range of ϕ values (e.g., 1−10^4 kPa^{-1} for 5.1 nm Ag

DOI: 10.1021/acscatal.8b01760
ACS Catal. 2018, 8, 11987−11998

clusters, 443 K, Figure 2b), as the CO*-to-O* coverage ratio varies gradually with ϕ. This coverage ratio also varies with temperature, ΔQ_{O-CO} (eq 1), and an entropic parameter (ΔS_{O-CO}, which is the difference between the entropies of O* and CO* adsorption), obtained by dividing eq 10a by 10b:

$$\left(\frac{[CO^*]}{[O^*]}\right)_{SS} = \frac{1}{K_{O-CO}\sqrt{\phi}} = \frac{1}{\exp\left(\frac{\Delta S_{O-CO}}{R}\right)\exp\left(\frac{\Delta Q_{O-CO}}{RT}\right)\sqrt{\phi}} \quad (11)$$

To capture this transition between the two kinetic regimes, we define a critical ϕ value, ϕ_t (subscript "t" denotes transition), at which the CO* and O* coverages both equal 0.5 ML and k^{first} acquires a half-order dependence on ϕ. This transition point occurs halfway between regimes 1 (first order) and 2 (zero order). This ϕ_t value depends on the reaction temperature as well as the ΔQ_{O-CO} and ΔS_{O-CO} of the metal:

$$\phi_t = \exp\left(-2\frac{\Delta S_{O-CO}}{R}\right)\exp\left(-2\frac{\Delta Q_{O-CO}}{RT}\right) \quad (12)$$

One would expect that the differences in the O* and CO* adsorption entropy (ΔS_{O-CO}) across all metals would remain insignificant, because of similar losses in translational and rotational degrees of freedom during adsorption. Taking this into consideration, $\Delta Q_{O-CO}T^{-1}$ becomes the sole parameter that dictates the critical ϕ_t value leading to the transition in kinetic regimes. Figure 6 shows this transition, as $\ln(\phi_t)$,

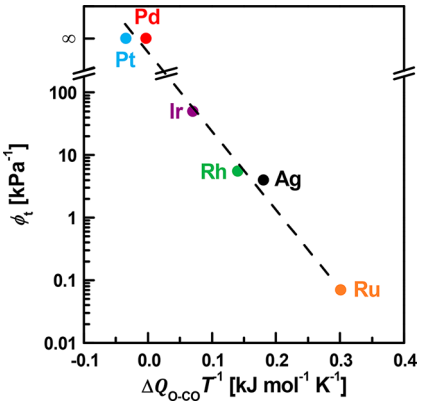

Figure 6. Values of ϕ_t parameter, which defines the midpoint of the transition between regimes 1 and 2 (from Figure 2), as a function of the difference in heats of O* and CO* adsorption on uncovered closed-packed terrace surfaces (Figure 1) divided by the reaction temperature, $\Delta Q_{O-CO}T^{-1}$ (eq 12), from data taken from the literature for Ru(0001)[7] (orange ●, 500 K), Rh(111)[7] (green ●, 500 K), and Ir(111)[16] (purple ●, 525 K), as well as our work for 9.3 nm Pd clusters (red ●, 400 K), 11.2 nm Pt clusters (blue ●, 453 K), and 5.1 nm Ag clusters (black ●, 443 K).

extracted from a variety of experimental data in Figure 2b, either generated from this work or obtained from the literature, as a linear function of $\Delta Q_{O-CO}T^{-1}$ for the entire series of metals (Pt, Pd > Ir > Rh > Ag > Ru). This linear relation between $\ln(\phi_t)$, a kinetic property, and $\Delta Q_{O-CO}T^{-1}$, a thermodynamic property, confirms the direct connection of CO oxidation kinetics to the difference in the heats of O* and CO* adsorption for the series of metals.

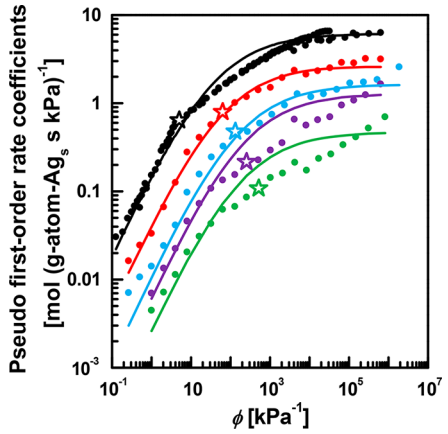

Figure 7. Pseudo-first-order rate coefficients ($k^{1st} = r_{CO}[CO]^{-1}$) for CO−$O_2$ reactions at 383 (green ●), 398 (purple ●), 413 (blue ●), 428 (red ●), and 443 K (black ●) on dispersed Ag (5 wt % Ag/SiO_2, 5.1 nm average Ag cluster diameter) and calculated rate coefficients using eq 6b (—) as a function of ϕ ((0.5−2) × 10^8 cm$^3_{STP}$ (g-atom of Ag$_s$)$^{-1}$ s^{-1}). Label ☆ indicates the midpoint of the transition between regimes 1 and 2 (ϕ_t) according to eqs 11 and 12.

3.4. Effects of Temperature on the Kinetic and Thermodynamic Parameters and Rate Coefficients for CO−O_2 Reactions on Dispersed Ag Clusters.

Figure 7 shows the first-order rate coefficients ($k^{1st} = r_{CO}[CO]^{-1}$) for Ag clusters (5.1 nm average diameter, 5 wt % Ag/SiO_2) plotted as a function of ϕ at several temperatures between 383 and 443 K. Over the entire temperature range, the rate coefficients exhibit the two distinct kinetic regimes (regimes 1 and 2) described in section 3.1. These rate coefficients at different temperatures all remain single-valued functions of the operating ϕ ratio, as captured by eq 6b, based on the values of the rate and equilibrium constants from nonlinear regressions of eq 5 against the rate data in Figure 7 (Table S1). As the operating ϕ value increases, the rate coefficients undergo a transition from regime 1 to regime 2. Taking the example at 443 K, their values increase linearly with ϕ at low ϕ values (0.13−1 kPa^{-1}) but become independent of ϕ at high ϕ values (>10^4 kPa^{-1}). As the reaction temperature increases from 383 to 443 K, the critical ϕ required for the transition between regimes 1 and 2 (ϕ_t, eq 12) decreases from 500 to 4 kPa^{-1}. This decrease in the ϕ_t values reflects an increasing preference for O*, instead of CO*, to occupy Ag sites at the higher temperatures, caused by the higher heat of adsorption for O* than for CO*, which is equivalent to a much higher temperature sensitivity of $K_{O_2}{}^{0.5}K_O{}^{0.5}$ than K_{CO}, and in turn, to a decrease in K_{O-CO} with increasing temperature.

Nonlinear regression of the rate data at the different temperatures (383−443 K) against eq 6a provides the groupings of kinetic and thermodynamic parameters ($k_{eff,1}$, $k_{eff,2}$, and K_{O-CO}) shown in Table 2 and the predicted rate coefficients from these parameters, shown as solid lines in Figure 7, that describe the trends for both regimes 1 and 2. Figure 3 shows these effective rate coefficients on Ag clusters together with those on Ru, Rh, Ir, Pd, and Pt clusters as a function of inverse temperature. In regime 1, the effective rate coefficients are larger on Ag than on Pt and Pd clusters over the temperature range 383−443 K (Figure 3a). The observed activation barrier for regime 1 ($E_{a,eff,1}$) reflects the barrier for CO*−O_2* reactions ($E_{a,CO-O_2}$) and the heats of O_2* and CO* adsorption (Q_{ads,O_2} and $Q_{ads,CO}$, respectively):

DOI: 10.1021/acscatal.8b01760
ACS Catal. 2018, 8, 11987−11998

$$E_{a,eff,1} = E_{a,CO-O_2} + Q_{ads,CO} - Q_{ads,O_2} \quad (13)$$

The value of $E_{a,eff,1}$ for 5.1 nm Ag clusters is 98 ± 7 kJ mol^{-1}. This observed barrier $E_{a,eff,1}$ is similar to those on 9.3 nm Pd and 1.2−20 nm Pt[10] clusters {84−97 kJ mol^{-1}}; it is smaller than those on 11.2 nm Pt clusters, Rh(111),[7] Pd(100),[8] and Pd(111)[9] {109−123 kJ mol^{-1}}. The differences among the barriers for these different metals and surface structures may reflect the different heats of adsorption on the metal surfaces according to eq 13. Despite the variation in these effective barriers (104 ± 20 kJ mol^{-1}), the rate constants on various Pd {9.3 nm clusters, Pd(100),[8] Pd(110),[16] Pd(111)[9]} and Pt {11.2 nm clusters, 1.2−20 nm clusters,[10] Pt(100)[16]} based catalysts appear to follow a single trend across a wide range of temperatures (Figure 3a, 373−695 K). These results reflect the structure insensitivity of the CO oxidation reaction on CO* covered surfaces, on which CO* adsorbates appear to significantly lower and thus remove the differences in the heat of CO* adsorption across these metals and also metals with different coordinations, as previously proposed for the cases of Pt[10] and Pd[42] clusters.

The effective rate coefficient in regime 2, $k_{eff,2}$, is larger on Ag than Ru clusters (383−443 K, Figure 3b). The activation barrier in regime 2, $E_{a,eff,2}$, reflects the barrier for CO*−O_2* reactions ($E_{a,CO-O_2}$) and the heats of O*, O_2*, and CO* adsorption ($Q_{ads,O}$, Q_{ads,O_2}, and $Q_{ads,CO}$ respectively), according to

$$E_{a,eff,2} = E_{a,CO-O_2} + 2Q_{ads,O} - Q_{ads,O_2} - Q_{ads,CO} \quad (14)$$

The $E_{a,eff,2}$ value is 51 ± 9 kJ mol^{-1} on 5.1 nm Ag clusters. This effective barrier ($E_{a,eff,2}$) on Ag clusters is smaller than that on Ru(0001) (84 kJ mol^{-1}).[7]

Finally, the temperature dependence of the equilibrium constant ratio (K_{O-CO}, eq 9) relates to the difference in the heats of O* and CO* adsorption (ΔQ_{O-CO}, eq 1), which through eqs 6b, 9, 13, and 14 also relates to the kinetic parameters for CO oxidation and, consequently, to the difference between the effective activation barriers in regimes 1 and 2:

$$K_{O-CO} = \exp\left(\frac{\Delta Q_{O-CO}}{RT}\right)\exp\left(\frac{\Delta S_{O-CO}}{R}\right) = \exp\left(\frac{E_{a,eff,2} - E_{a,eff,1}}{2RT}\right) \quad (15)$$

The value of ΔQ_{O-CO}, extracted from the rate data at different temperatures (Figure 7) and eq 15, is −24 ± 5 kJ mol^{-1}. The ΔQ_{O-CO} value derived from the rate data fittings (−24 ± 5 kJ mol^{-1}) is smaller than that derived from the equilibrium O_2 and CO uptakes (2 kJ mol^{-1}, section 3.3) and much smaller than the value determined from DFT calculations for O*[18] and CO*[14] adsorption on uncovered Ag(111) surfaces (80 kJ mol^{-1}, Figure 1). Since Ag cluster surfaces are nearly saturated with CO* and O* during steady-state reactions, the negative and much smaller ΔQ_{O-CO} suggests that lateral repulsive interactions between the O* and CO* adsorbates lower the heat of O* adsorption much more significantly than the heat of CO* adsorption.

3.5. Effects of Mean Ag Cluster Size and Average Ag Surface Coordination on CO Turnover Rates. As the cluster size increases, the average coordination of Ag sites increases and, as a result, their affinity to bind with adsorbates decreases. Such changes may affect the coverages, the energies of adsorbed intermediates and transition state, and in turn, the kinetic and thermodynamic parameters in the rate expression of eq 6a. We probe the catalytic effects of Ag surface coordination, by measuring CO turnover rates on a series of catalysts with varying mean Ag cluster diameters between 3.1 and 29.3 nm and over the entire ϕ range ((0.13−6.4) × 10^5 kPa^{-1}), covering both regimes 1 and 2 and the transition between them.

Figure 8 shows the rate coefficients $k_{eff,1}$ and $k_{eff,2}$ for regimes 1 and 2 (eqs 7 and 8), respectively, and the thermodynamic parameter K_{O-CO} (eq 9) at 443 K, plotted as a function of mean Ag cluster diameters. These rate and thermodynamic parameters were determined from nonlinear regression of the rate data from the series of catalysts against eq 6a. As Ag cluster size increases from 3.1 to 5.1 nm, the effective rate coefficient $k_{eff,1}$ in regime 1 ($k_{eff,1}$) first increases by 5-fold from 0.04 to 0.22 g-atom of Ag_s s^{-1} kPa^{-1}. Above 5.1 nm, the $k_{eff,1}$ value decreases markedly by 50-fold to 0.004 g-atom of Ag_s s^{-1} kPa^{-1}. As the mean Ag cluster diameter increases from 3.1 to 29.3 nm, both the equilibrium constants of O_2 and CO adsorption (K_{O_2} and K_{CO}) decrease in response to the weaker O_2* and CO* bindings to the clusters as the fractions of coordinatively unsaturated edge sites decrease from 0.30 to 0.03, while those of corner sites rapidly decrease from 0.05 to 0.0004 (shown in Table S3 of the Supporting Information).[43] Here, K_{O_2} seemingly decreases more significantly than K_{CO}, indicating that the O_2 adsorption has a stronger cluster size dependence than that of CO, thus resulting in an overall decrease in the $K_{O_2}(K_{CO})^{-1}$ ratio with increasing cluster diameter. At the same time, the rate constants for CO*−O_2* reactions (k_{CO-O_2}) increase because the more weakly bound CO* prevalent on the larger Ag clusters is able to bind more strongly to the O atom of O_2* at the transition state, thus lowering the activation free energies. Therefore, the initial increase in $k_{eff,1}$ value with Ag cluster diameter up to 5.1 nm suggests that the increase in k_{CO-O_2} is larger than and compensates for the decrease in the $K_{O_2}(K_{CO})^{-1}$ ratio. For Ag clusters larger than 5.1 nm, the

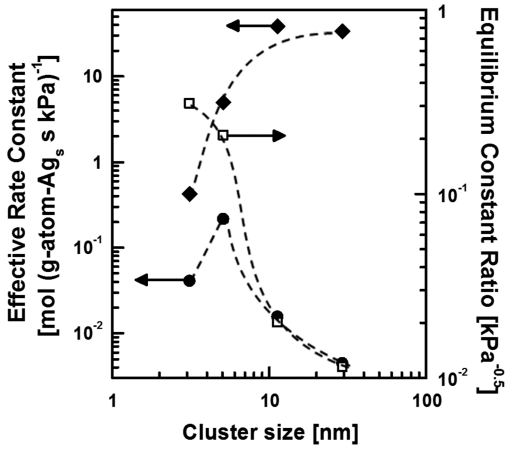

Figure 8. Effective rate constants $k_{eff,1}$ (●, regime 1, eq 7) and $k_{eff,2}$ (◆, regime 2, eq 8) and equilibrium constant ratio K_{O-CO} (□, eq 9) obtained from nonlinear regression of rate data against the proposed rate expression (eq 6a) for CO−O_2 reactions at 443 K on dispersed Ag clusters (1−5 wt % Ag/SiO_2), plotted as a function of Ag mean cluster diameters (ϕ = (0.13−6.4) × 10^5 kPa^{-1}, (0.5−2) × 10^8 cm$^3_{STP}$ (g-atom of Ag_s)$^{-1}$ s^{-1}).

DOI: 10.1021/acscatal.8b01760
ACS Catal. 2018, 8, 11987−11998

fraction of coordinatively unsaturated sites becomes exceptionally small and the k_{CO-O_2} increase is much less significant when comparing to the decrease in the $K_{O_2}(K_{CO})^{-1}$ ratio. For this reason, $k_{eff,1}$ values decrease for clusters above 5.1 nm.

In regime 2, the effective rate coefficient $k_{eff,2}$ increases by 2 orders of magnitude, i.e., from 0.42 to 39 g-atom of Ag_s s^{-1} kPa^{-1}, as the Ag cluster diameter increases from 3.1 to 11.3 nm, after which it remains nearly constant at 36 ± 3 mol (g-atom of Ag_s s kPa)$^{-1}$, insensitive to any further increase in the Ag diameter. The initial increase of the $k_{eff,2}$ value with Ag diameter is likely a result of a significant increase in k_{CO-O_2}, while the $K_{CO}(K_O)^{-1}$ ratio remains relatively constant due to the strong binding of both CO* and O* to surface Ag atoms and their similar dependence on the Ag diameter. As the Ag diameter increases to above 11.3 nm, k_{CO-O_2} becomes nearly invariant with cluster diameter since the fraction of active sites at terraces approaches unity (0.93−0.97) and most sites remain highly coordinated (shown in Table S3 of the Supporting Information),[43] leading to the nearly constant $k_{eff,2}$ values.

Included in Figure 8 is the thermodynamic parameter K_{O-CO}, which reflects the difference in the heats of O* and CO* adsorption (ΔQ_{O-CO}, eq 9). Its value sharply decreases by 30-fold from 0.31 to 0.01 $kPa^{-0.5}$ with increasing cluster diameter, an indication that the heat of O* adsorption decreases much more sensitively than that of CO* adsorption. In other words, the larger Ag clusters prefer to bind to CO* instead of O*, when comparing to the smaller Ag clusters. These observations agree with the DFT calculated changes in the heats of O* and CO* adsorption in response to changing coordinative unsaturation. For example, the heat of O_2* adsorption decreases from 352 to 271 kJ mol^{-1}, as the Pt coordination number changes from 8 on (100) terraces to 9 on (111) terraces. In contrast, the heat of CO* adsorption decreases by a much smaller magnitude on the same surfaces, from 140 to 120 kJ mol^{-1}, in response to changing coordination numbers from 8 to 9.[10]

4. CONCLUSIONS

Rate measurements in the kinetically controlled regime and equilibrium uptakes of oxygen and carbon monoxide lead to a proposed reaction pathway for carbon monoxide oxidation on supported Ag clusters. During steady-state catalysis, Ag cluster surfaces remain nearly saturated with CO* and O* with their relative abundance depending on the operating ratio of O_2 pressure to the square of CO pressure. On these surfaces, CO* reacts with a small number of molecular O_2* in a kinetically relevant step. At low $[O_2]$-to-$[CO]^2$ ratios, the most abundant surface intermediates are CO* and the first-order rate coefficients in CO increase linearly with these ratios. As the pressure ratio increases, the identity of the most abundant surface intermediate undergoes a transition from CO* to O*, causing the first-order rate coefficients to become independent of the pressure ratio. The transition in the kinetic dependencies, caused by the changes in the relative coverages of CO* and O*, is general for Ag, Rh, Ru, and Ir metal catalysts; the $[O_2]$-to-$[CO]^2$ ratios that lead to the transition in kinetic regimes appear to vary with the difference in the heats of O* and CO* adsorption for these metals.

On surfaces predominantly covered with CO*, the effective CO rate coefficients are similar on Ru, Rh, Ir, Pd, and Ag, and smaller on Pt metal catalysts. On surfaces covered with O*, the effective rate coefficients on Rh, Ir, and Ag are similar, while those on Ru metals are smaller. CO oxidation effective rate coefficients in the CO* covered regime first increase and then decrease with increasing Ag cluster size. The initial increase in effective rate coefficients arises due to the more weakly bound and thus reactive CO* and O_2*, which are prevalent on the larger Ag clusters. As cluster diameter increases further, the rate coefficients decrease, indicating that the heat of O_2* adsorption decreases to a much larger extent than the heat of CO* adsorption. The structure sensitivity effects suggest that larger Ag clusters prefer binding to CO* instead of O*.

■ ASSOCIATED CONTENT

Supporting Information

The Supporting Information is available free of charge on the ACS Publications website at DOI: 10.1021/acscatal.8b01760.

CO−O_2 rate data; derivation of rate expressions; sensitivity analysis of rate parameters; O_2 and CO uptake data (PDF)

■ AUTHOR INFORMATION

Corresponding Author

*E-mail: cathy.chin@utoronto.ca. Tel.: (416) 978-8868. Fax: (416) 978-8605.

ORCID

Ya-Huei Cathy Chin: 0000-0003-4388-0389

Notes

The authors declare no competing financial interest.

■ ACKNOWLEDGMENTS

This study was supported by the Natural Sciences and Engineering Research Council of Canada and the Canada Foundation for Innovation. We also acknowledge the Queen Elizabeth II Graduate Scholarships in Science & Technology and the Ontario Graduate Scholarships awarded to Petar T. Lachkov. We thank Haoyu Nie for carrying out the CO−O_2 rate measurements on Pd and Pt clusters.

■ REFERENCES

(1) Gandhi, H. S.; Graham, G. W.; McCabe, R. W. Automotive Exhaust Catalysis. *J. Catal.* **2003**, *216*, 433−442.

(2) Muraki, H.; Matunaga, S.-I.; Shinjoh, H.; Wainwright, M. S.; Trimm, D. L. The Effect of Steam and Hydrogen in Promoting the Oxidation of Carbon Monoxide over a Platinum on Alumina Catalyst. *J. Chem. Technol. Biotechnol.* **1991**, *52*, 415−424.

(3) Oh, S. H.; Eickel, C. C. Influence of Metal Particle Size and Support on the Catalytic Properties of Supported Rhodium: CO-O_2 and CO-NO Reactions. *J. Catal.* **1991**, *128*, 526−536.

(4) Liotta, L. F.; Di Carlo, G.; Pantaleo, G.; Venezia, A. M. Supported Gold Catalysts for CO Oxidation and Preferential Oxidation of CO in H_2 Stream: Support Effect. *Catal. Today* **2010**, *158*, 56−62.

(5) Ojeda, M.; Zhan, B.-Z.; Iglesia, E. Mechanistic Interpretation of CO Oxidation Turnover Rates on Supported Au Clusters. *J. Catal.* **2012**, *285*, 92−102.

(6) Saavedra, J.; Powell, C.; Panthi, B.; Pursell, C. J.; Chandler, B. D. CO Oxidation over Au/TiO_2 Catalyst: Pretreatment Effects, Catalyst Deactivation, and Carbonates Production. *J. Catal.* **2013**, *307*, 37−47.

(7) Goodman, D. W.; Peden, C. H. F. Carbon Monoxide Oxidation over Rhodium and Ruthenium: A Comparative Study. *J. Phys. Chem.* **1986**, *90*, 4839−4843.

DOI: 10.1021/acscatal.8b01760
ACS Catal. 2018, 8, 11987−11998

(8) Szanyi, J.; Goodman, D. W. CO Oxidation on Palladium. 1. A Combined Kinetic-Infrared Reflection Absorption Spectroscopic Study of Pd(100). *J. Phys. Chem.* **1994**, *98*, 2972−2977.
(9) Szanyi, J.; Kuhn, W. K.; Goodman, D. W. CO Oxidation on Palladium. 2. A Combined Kinetic-Infrared Reflection Absorption Spectroscopic Study of Pd(111). *J. Phys. Chem.* **1994**, *98*, 2978−2981.
(10) Allian, A. D.; Takanabe, K.; Fujdala, K. L.; Hao, X.; Truex, T. J.; Cai, J.; Buda, C.; Neurock, M.; Iglesia, E. Chemisorption of CO and Mechanism of CO Oxidation on Supported Platinum Nanoclusters. *J. Am. Chem. Soc.* **2011**, *133*, 4498−4517.
(11) García-Diéguez, M.; Iglesia, E. Structure Sensitivity via Decoration of Low-Coordination Exposed Metal Atoms: CO Oxidation Catalysis on Pt Clusters. *J. Catal.* **2013**, *301*, 198−209.
(12) Chin, Y.-H. C.; Buda, C.; Neurock, M.; Iglesia, E. Selectivity of Chemisorbed Oxygen in C−H Bond Activation and CO Oxidation and Kinetic Consequences for CH_4-O_2 Catalysis on Pt and Rh Clusters. *J. Catal.* **2011**, *283*, 10−24.
(13) Royer, S.; Duprez, D. Catalytic Oxidation of Carbon Monoxide over Transition Metal Oxides. *ChemCatChem* **2011**, *3*, 24−65.
(14) Grabow, L. C.; Hvolbæk, B.; Nørskov, J. K. Understanding Trends in Catalytic Activity: The Effect of Adsorbate−Adsorbate Interactions for CO Oxidation Over Transition Metals. *Top. Catal.* **2010**, *53*, 298−310.
(15) Chin, Y.-H. C.; Buda, C.; Neurock, M.; Iglesia, E. Reactivity of Chemisorbed Oxygen Atoms and Their Catalytic Consequences during CH_4-O_2 Catalysis on Supported Pt Clusters. *J. Am. Chem. Soc.* **2011**, *133*, 15958−15978.
(16) Berlowitz, P. J.; Peden, C. H. F.; Goodman, D. W. Kinetics of Carbon Monoxide Oxidation on Single-Crystal Palladium, Platinum, and Iridium. *J. Phys. Chem.* **1988**, *92*, 5213−5221.
(17) Haruta, M.; Tsubota, S.; Kobayashi, T.; Kageyama, H.; Genet, M. J.; Delmon, B. Low-Temperature Oxidation of CO over Gold Supported on TiO_2, α-Fe_2O_3, and Co_3O_4. *J. Catal.* **1993**, *144*, 175−192.
(18) Van Santen, R. A.; Neurock, M. *Molecular Heterogeneous Catalysis*; Wiley-VCH: Weinheim, 2006.
(19) Imbihl, R.; Cox, M. P.; Ertl, G.; Müller, H.; Brenig, W. Kinetic Oscillations in the Catalytic CO Oxidation on Pt(100): Theory. *J. Chem. Phys.* **1985**, *83*, 1578−1587.
(20) Imbihl, R.; Cox, M. P.; Ertl, G. Kinetic Oscillations in the Catalytic CO Oxidation on Pt(100): Experiments. *J. Chem. Phys.* **1986**, *84*, 3519−3534.
(21) Bassett, M. R.; Imbihl, R. Mathematical Modeling of Kinetic Oscillations in the Catalytic CO Oxidation on Pd(110): The Subsurface Oxygen Model. *J. Chem. Phys.* **1990**, *93*, 811−821.
(22) Sandoval, A.; Aguilar, A.; Louis, C.; Traverse, A.; Zanella, R. Bimetallic Au−Ag/TiO_2 Catalyst Prepared by Deposition−Precipitation: High Activity and Stability in CO Oxidation. *J. Catal.* **2011**, *281*, 40−49.
(23) Afanasev, D. S.; Yakovina, O. A.; Kuznetsova, N. I.; Lisitsyn, A. S. High Activity in CO Oxidation of Ag Nanoparticles Supported on Fumed Silica. *Catal. Commun.* **2012**, *22*, 43−47.
(24) Yen, C.-W.; Lin, M.-L.; Wang, A.; Chen, S.-A.; Chen, J.-M.; Mou, C.-Y. CO Oxidation Catalyzed by Au−Ag Bimetallic Nanoparticles Supported in Mesoporous Silica. *J. Phys. Chem. C* **2009**, *113*, 17831−17839.
(25) Liu, X.; Wang, A.; Yang, X.; Zhang, T.; Mou, C.-Y.; Su, D.-S.; Li, J. Synthesis of Thermally Stable and Highly Active Bimetallic Au−Ag Nanoparticles on Inert Supports. *Chem. Mater.* **2009**, *21*, 410−418.
(26) Wang, A.-Q.; Chang, C.-M.; Mou, C.-Y. Evolution of Catalytic Activity of Au−Ag Bimetallic Nanoparticles on Mesoporous Support for CO Oxidation. *J. Phys. Chem. B* **2005**, *109*, 18860−18867.
(27) Tang, D.; Chen, Z.; Hu, J.; Sun, G.; Lu, S.; Hu, C. CO Oxidation Catalyzed by Silver Nanoclusters: Mechanism and Effects of Charge. *Phys. Chem. Chem. Phys.* **2012**, *14*, 12829.
(28) Negreiros, F. R.; Sementa, L.; Barcaro, G.; Vajda, S.; Aprá, E.; Fortunelli, A. CO Oxidation by Subnanometer Ag_xAu_{3-x} Supported Clusters via Density Functional Theory Simulations. *ACS Catal.* **2012**, *2*, 1860−1864.
(29) Wei, Z.-Z.; Li, D.-C.; Pang, X.-Y.; Lv, C.-Q.; Wang, G.-C. The Mechanism of Low-Temperature CO Oxidation on IB Group Metals and Metal Oxides. *ChemCatChem* **2012**, *4*, 100−111.
(30) Lei, X.; Mbamalu, G.; Qin, C. CO Oxidation by Molecular and Atomic Oxygen on Ag(100): A Density Functional Theory Study. *J. Phys. Chem. C* **2017**, *121*, 2635−2642.
(31) Bergeret, G.; Gallezot, P. Particle Size and Dispersion Measurements. In *Handbook of Heterogeneous Catalysis*; Wiley-VCH: Weinheim, 2008; pp 738−765.
(32) Czanderna, A. W. The Adsorption of Oxygen on Silver. *J. Phys. Chem.* **1964**, *68*, 2765−2771.
(33) Lide, D. R. *CRC Handbook of Chemistry and Physics*, 78th ed.; CRC Press: Boca Raton, FL, 1997.
(34) Valden, M.; Lai, X.; Goodman, D. W. Onset of Catalytic Activity of Gold Clusters on Titania with the Appearance of Nonmetallic Properties. *Science* **1998**, *281*, 1647−1650.
(35) Aguilar-Guerrero, V.; Gates, B. C. Kinetics of CO Oxidation Catalyzed by Supported Gold: A Tabular Summary of the Literature. *Catal. Lett.* **2009**, *130*, 108.
(36) Campbell, C. T.; Sellers, J. R. V. The Entropies of Adsorbed Molecules. *J. Am. Chem. Soc.* **2012**, *134*, 18109−18115.
(37) McElhiney, G.; Papp, H.; Pritchard, J. The Adsorption of Xe and CO on Ag(111). *Surf. Sci.* **1976**, *54*, 617−634.
(38) Shustorovich, E. The Bond-Order Conservation Approach to Chemisorption and Heterogeneous Catalysis: Applications and Implications. *Adv. Catal.* **1990**, *37*, 101−163.
(39) Johnson, R. D., III. *NIST Computational Chemistry Comparison and Benchmark Database, NIST Standard Reference Database Number 101*, release 17b; 2015. http://cccbdb.nist.gov/.
(40) Smeltzer, W. W.; Tollefson, E. L.; Cambron, A. Adsorption of Oxygen by a Silver Catalyst. *Can. J. Chem.* **1956**, *34*, 1046−1060.
(41) Benton, A. F.; Drake, L. C. Kinetics of Reaction and Adsorption in the System Silver—Oxygen. *J. Am. Chem. Soc.* **1934**, *56*, 255−263.
(42) Ladas, S.; Poppa, H.; Boudart, M. The Adsorption and Catalytic Oxidation of Carbon Monoxide on Evaporated Palladium Particles. *Surf. Sci.* **1981**, *102*, 151−171.
(43) Van Hardeveld, R.; Hartog, F. The Statistics of Surface Atoms and Surface Sites on Metal Crystals. *Surf. Sci.* **1969**, *15*, 189−230.

DOI: 10.1021/acscatal.8b01760
ACS Catal. 2018, 8, 11987−11998